ADVANCES IN ATMOSPHERIC SCIENCES, VOL. 26, NO. 2, 2009, 192–201

Impact of Global SST on Decadal Shift of East Asian Summer Climate

FU Jianjian[1,2] (付建建), LI Shuanglin*[2] (李双林), and LUO Dehai[1] (罗德海)

[1] *College of Physical and Environmental Oceanography, Ocean University of China, Qingdao* 266100

[2] *Nansen-Zhu International Research Centre (NZC), Institute of Atmospheric Physics, Chinese Academy of Sciences, Beijing* 100029

(Received 1 November 2007; revised 26 February 2008)

ABSTRACT

East Asia experienced a significant interdecadal climate shift around the late 1970s, with more floods in the valley of the Yangtze River of central-eastern China and more severe drought in North China since then. Whether global SST variations have played a role in this shift is unclear. In the present study, this issue is investigated by ensemble experiments of an atmospheric general circulation model (AGCM), the GFDL AM2, since one validation reveals that the model simulates the observed East Asian Summer Monsoon (EASM) well. The results suggest that decadal global SST variations may have played a substantial role in this climate shift. Further examination of the associated atmospheric circulation shows that these results are physically reasonable.

Key words: East Asian summer monsoon, interdecadal shift, SST, AGCM

Citation: Fu, J. J., S. Li, and D. H. Luo, 2009: Impact of global SST on decadal shift of East Asian summer climate. *Adv. Atmos. Sci.*, **26**(2), 192–201, doi: 10.1007/s00376-009-0192-z.

1. Introduction

East Asia is a typical monsoon area, where industrial and agricultural production and human life are substantially influenced by the anomalous activity of monsoons, especially in summer. Predicting the East Asian Summer Monsoon (EASM) is of utmost importance to the East Asian countries and is the key topic of the climate practical and research community. EASM features various time-scales. In addition to year-to-year variations, it also varies on the decadal time-scale. For instance, one significant interdecadal summer climate shift occurred around the late 1970s, with more floods in central-eastern China along with more severe drought in North China since then (e.g., Huang, 2001; Wang, 2001; Zhou and Yu, 2006; Ding et al., 2007). It has brought challenges to sustainable development in the country, but the underlying mechanism has not been completely understood until now. Clarifying its formation is not only important for historical climate attribution, but also constitutes a premise for projecting the future climate change of the region.

It is known that the global oceans are playing important roles in the climate system because of its large heat inertia and the slow movement of sea water. An interdecadal warming of global SST was observed (Fig. 1a), especially in the tropical Indian Ocean (Hoerling et al., 2004) and the tropical eastern Pacific (e.g., Nitta and Yamada, 1989; Zhang et al., 1997). To what extent global historical SST evolutions have been responsible for the interdecadal climate shift is intriguing but unclear, and has attracted recent research interests. As for the tropical SST, Gong and Ho (2002) and Huang (2001) documented that the ENSO-like decadal warming in the tropical central-eastern Pacific may be the cause of the climate shift. Yang et al. (2007) found that interannual tropical Indian Ocean basin warming can influence the lower-tropospheric southwesterly wind over the Indian Ocean and the upper-tropospheric South Asia High (SAH), subsequently affecting the EASM. Thus, the tropical Indian Ocean may also have played a role in the climate shift due to its substantial interdecadal warming which is especia-

*Corresponding author: LI Shuanglin, shuanglin.li@mail.iap.ac.cn

lly clear when compared to the interannual SST standard deviation (Fig. 1b). As for the extratropical oceans, the North Pacific SST, particularly its decadal fluctuation pattern coined as Pacific Decadal Oscillation (PDO), may be an important cause of this climate shift (Li and Xian, 2003; Yang and Zhang, 2003). Yang et al. (2005) found the persistence of North China summer rainfall is well related to the PDO. During its warm phase, the tropical central-eastern Pacific is warmer while the northwestern North Pacific is cooler, which favors suppressed rainfall in North China. It is opposite during its cold phase. Recently, Wu and Zhang (2007) found an interdecadal shift in the late 1980s in both the North Pacific SST and the summer rainfall in South China, supporting the PDO influence. In addition, the North Atlantic SST may also exert influence. Lu and Dong (2005) found that the North Atlantic SST has played an important role in the climate of the year 1997/98—the warmest year in the 20th century in China. Lu et al. (2006) and Li and Bates (2007) conducted observational analyses, and coupled or uncoupled atmospheric general circulation model (AGCM) experiments, and found that the Atlantic Multidecadal Oscillation (AMO), the multidecadal basin-scale warming or cooling of the North Atlantic, exerts significant influence on both the EASM and East Asian winter monsoon, respectively.

However, one puzzling finding is that the SST influence that was hinted in previous observational studies has not been confirmed by AGCM experiments. Han and Wang (2007) forced an AGCM, IAP9L, with prescribed historical-evolving global SST and sea ice concentration, and found that the interdecadal climate shift cannot be reproduced. Thus, they concluded that the climate shift may have originated either from atmospheric internal variability or from other natural forcings rather than the global SST or sea ice variations. Such a conclusion is considerably uncertain and warrants further verification due to the fact that their ensemble size is very limited (with only 4 members). This motivates the present modeling study.

One AGCM, the Atmospheric Model version 2.0 of the Geophysical Fluid Dynamics Laboratory (GFDL AM2 in brief, hereafter) of the National Oceanic and Atmospheric Administration (NOAA) of the United Sates are employed to conduct ensemble experiments. The paper is organized as follows. Section 2 describes the model experiment design and the datasets used. Section 3 validates the model's simulations of the EASM. In section 4, the modeled results concerning

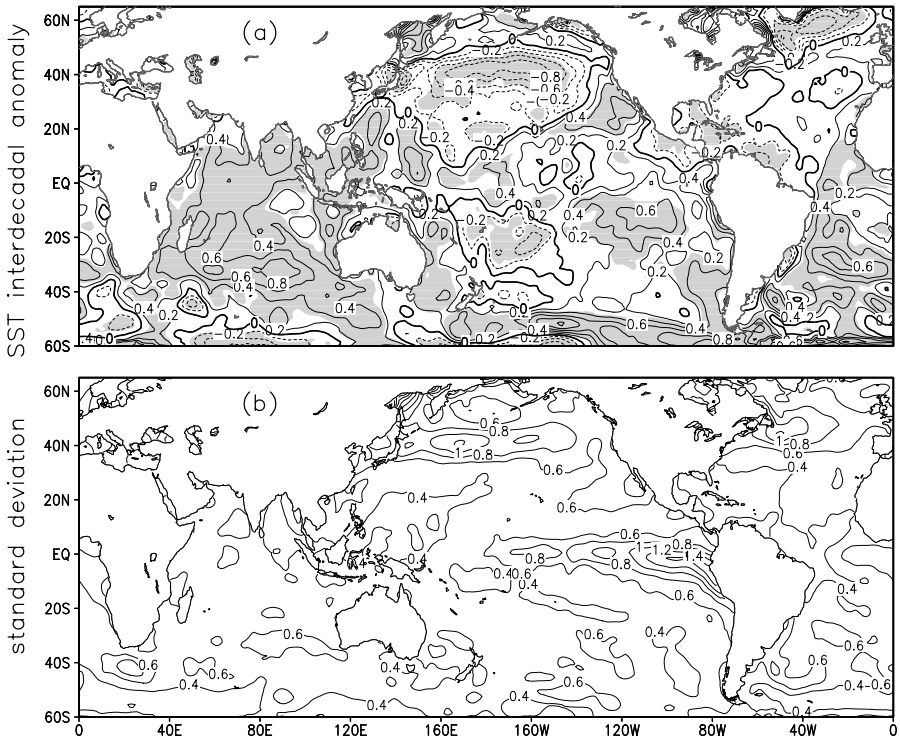

Fig. 1. (a) The difference of the climatogical mean July–August SST (Units: °C) calculated from 1979–1998 minus those from 1950–1969. The shaded areas indicate significance at the 95% level. (b) The July–August mean of monthly SST standard deviation (Units: °C) calculated from 1950–1998.

the influence of global SST variations on the East Asian interdecadal climate shift are presented. A summary along with concluding remarks are presented in the last section.

2. Model experiment design and datasets

2.1 *Model and experiments*

The GFDL AM2 was developed and released recently. It includes a new dynamic gridpoint core (Arakawa B-grid), a fully prognostic cloud scheme, a moist turbulence scheme, and a multi-species three-dimensional aerosol climatology, as well as components from the previous GFDL AGCM versions. A detailed description can be found in GAMT (2004).

A total of two sets of ensemble experiments, each of which constitutes 2 runs, are performed. In the first ensemble, run one is formed by integrating the AM2 for a 25-year period with the climatological mean SST seasonal cycle as the boundary forcing. The climatological SST is derived from the 20-year mean monthly SSTs in 1950–1969 in the GISST dataset (Rayner et al., 1996). Run two is the same except that one of the initial fields used is different. For both the two runs, the first year is discarded as the model's spin-up period, and thus a total of 48 model years are available. Since the oceanic boundary forcing is the climatological mean SST, the present ensemble should correspond to that with 48 members, each of which is integrated for one year. The second set of ensembles is the same except that a different climatological SST seasonal cycle, the mean through 1979–1998, is used. Since the only difference between these two sets of ensembles is the SST climatology (Fig. 1), the difference of modeled atmospheric mean state between them should represent the influence of different SST climatology if the role of SST transience is neglected. Subsequently, these experiments can be used to investigate the decadal SST influence on the EASM decadal climate shift which occurred around the late 1970s.

2.2 *Datasets*

The CMAP (Climate Prediction Center Merged Analysis of Precipitation) global monthly rainfall da-

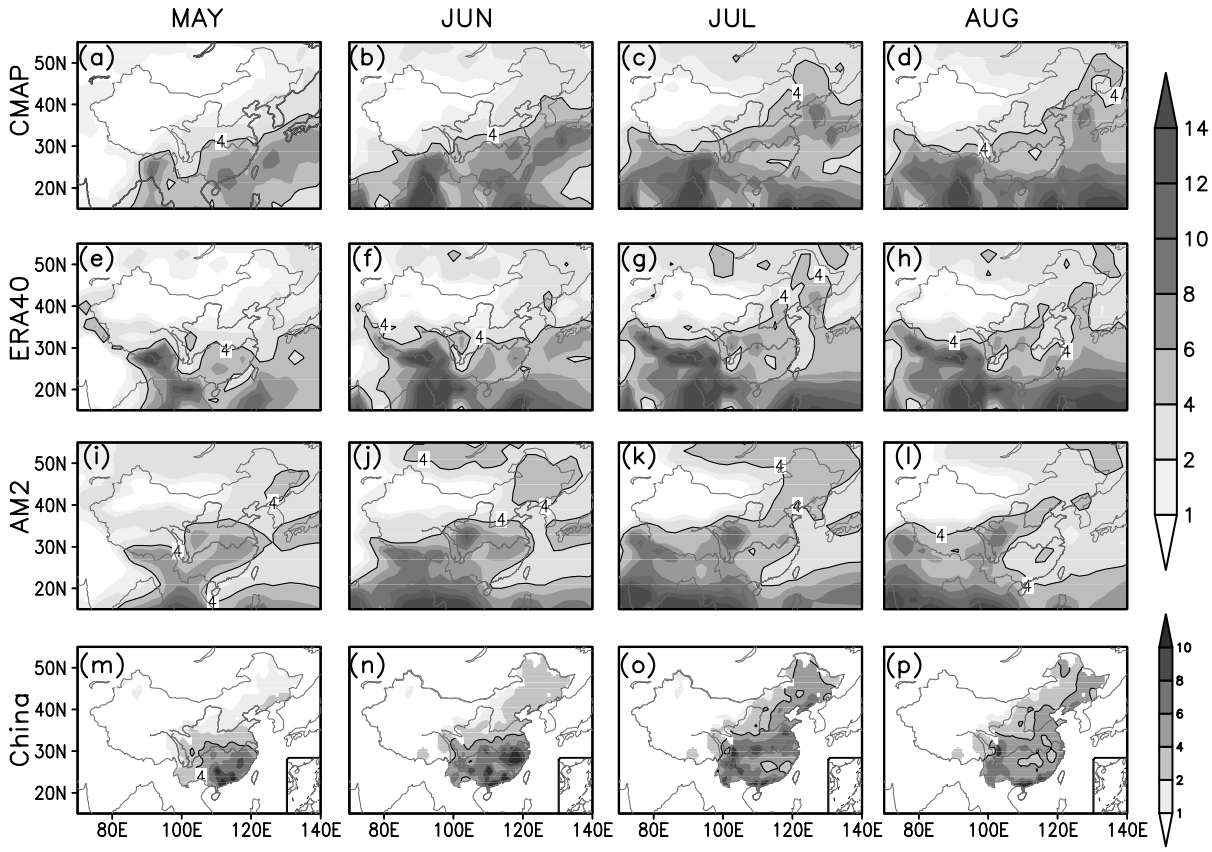

Fig. 2. Climatological summer monthly precipitation in the CMAP (a, b, c, d), the ERA-40 (e, f, g, h), the AM2 (i, j, k, l), and the 160 station observations in China (m, n, o, p). The columns from left to right correspond to May, June, July, and August, individually. The solid line in each indicates the contour of 4 mm d^{-1}.

taset (Xie and Arkin, 1997) is used to verify the AM2 simulated large-scale rainfall climatology. Because the beginning date of this CMAP dataset is only from 1979, it is not long enough for the decadal climate issues. Instead, a more reliable dataset, the gauged precipitation from 160 stations in China beginning in 1951, is used when studying the interdecadal climate shift.

Monthly 100-hPa and 500-hPa geopotential height, 850-hPa horizontal wind (u and v) from the NCEP-NCAR (the National Centers for Environmental Prediction-National Center for Atmosphere Research) reanalysis (Kalnay et al., 1996) and the ECMWF (European Center for Medium-Range Weather Forecasts) 40-yr reanalysis (ERA-40) (Upplal et al., 2004) are used to understand the circulation variations associated with the interdecadal shift of EASM. The former begins from January 1948 while the latter from September 1957. The purpose of using both sets of reanalysis datasets at the same time is to provide a comparison reference for each other, in view of the poor quality prior to 1979 in the southern hemisphere in the NCEP/NCAR reanalysis (Renwick, 2002) and the short record length of the ERA-40.

3. Validation of the EASM in the AM2

Whether one model simulates atmospheric response to one forcing in the same way as in the real world depends considerably on the model's ability in simulating observed atmospheric variability. One model with unrealistic intrinsic variability tends to yield a distorted response. The ability of the AM2 in simulating EASM is validated first. The distribution and seasonal march of the model's precipitation as well as several key EASM sub-systems including the SAH, the Western Pacific Subtropical High (WPSH) and the cross-equator air streams, are compared with observational datasets for both the NCEP-NCAR and the ERA-40 reanalyses.

Figure 2 shows the seasonal march of climatogical monthly precipitation during the summer from May to August. The AM2's rainfall climatology is represented by the climatological mean from the second ensemble (with boundary forcing of the climatological SST derived from the mean through 1979–1998), while the climatology for the other datasets is calculated as the mean from 1979 to 1998. As far as large-scale rainfall is concerned, the AM2 bears resemblance to both the CMAP and the ERA-40, albeit being uniformly weaker in every month. The homogeneously less rainfall in the AM2, the ERA-40 and the CMAP in comparison with the gauged rainfall of 160 stations in China may be associated with AGCM deficiency in resolving the complicated topography in the region of China. All three of these datasets should have incorporated the influence from at least one AGCM with

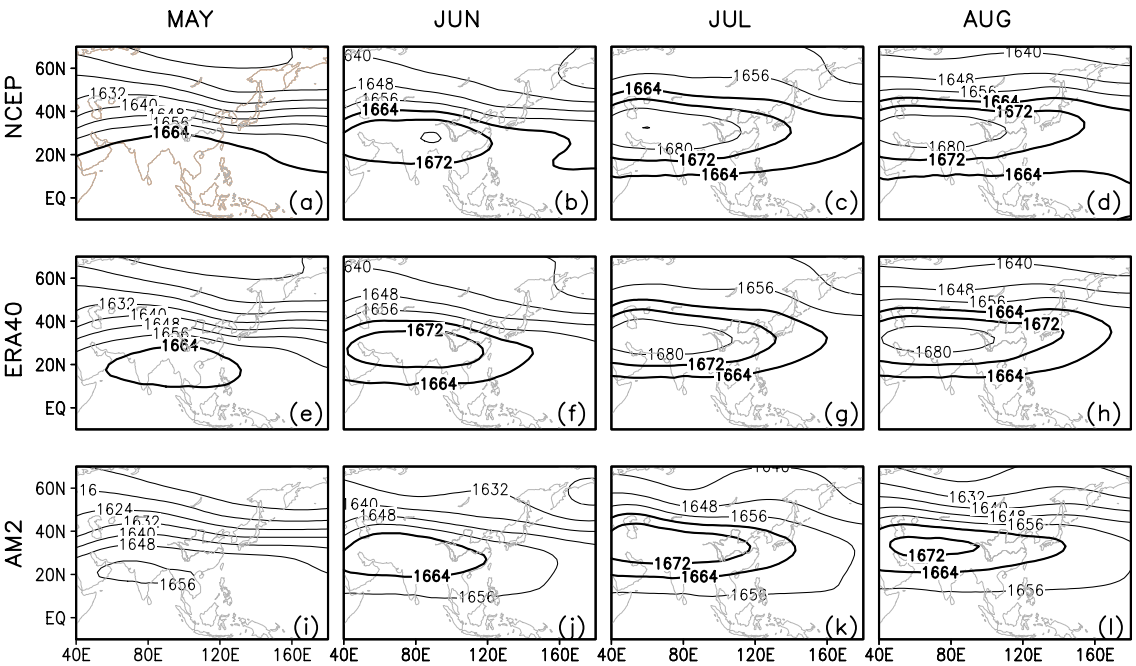

Fig. 3. (a, b, c, and d) Climatological summer monthly 100-hPa geopotential height from the NCEP-NCAR reanalysis. (e, f, g, and h) and (i, j, k, and l), as (a, b, c, and d), but from the ERA-40 and the AM2, respectively. The columns from left to right correspond to May through August, respectively, indicating the seasonal march in summer. Contour intervals are 8 dagpm.

the AGCM's application in a reanalysis in consideration. As far as the seasonal evolution is concerned, the AM2 largely reproduces the observed. For example, there is strong rainfall in eastern India north of the Bay of Bengal (BOB) and in the Indochina Peninsula in May, meanwhile South China is at the edge of the main rainfall belt with significant rainfall. Along with the season march from June to July, the dominant rainfall belt moves northward and is locates in the Yangtze River valley of central-eastern China. In August, the rain belt extends further northward and reaches North and Northeast China. Hence, these comparisons suggest that the AM2 reasonably reproduces the observed summer rainfall distribution and seasonality. This point is consistent with the fact that the model simulates the EASM sub-systems well, as is seen below.

Figure 3 shows climatological monthly 100-hPa geopotential height in summer months, since the SAH in the upper troposphere is one of the primary EASM sub-systems and plays an important role in modulating seasonal march of EASM (Tao et al., 1957). First, the shape and seasonality of the SAH in both reanalyses bear a considerable visual consistency, albeit the values in the ERA-40 are somewhat smaller. Second, the behavior of the SAH in the AM2 resembles both sets of reanalyses well. For instance, along with the seasonal march from May toward August, the contour lines of 1664 and 1672 expand eastward and the latitudinal location of the long axis of their enclosed ellipse moves to the north. Also, in mid-summer (July and August) the longitudinal location of the SAH in the AM2 is anchored nearly the same as in both the ERA-40 and the NCEP/NCAR, albeit the AM2 geopotential height are systematic smaller which is related to systematic errors of the AM2 (GAMT, 2004).

Figure 4 shows climatological monthly 500-hPa geopotential height, which is used to verify the activity of the WPSH. First, a considerable consistency of the seasonal march of 500-hPa geopotential height between the two reanalyses is clearly seen from the evolution of the characteristic contours of 584 and 588, albeit the geopotential height values in the NCEP/NCAR reanalysis is somewhat smaller, in contrary with the bias at 100 hPa. Second, the AM2 largely reproduces the seasonal evolution of the WPSH. For example, the ridge line (zero westerly location at 120°E) of contour 584 is at 15°N in May, moves to the north gradually in June and July, and arrives at 30°N in August. Correspondingly, the area encircled by 586 increases from May to August.

Lower-tropospheric cross-equator air streams are another key EASM sub-system (Tao et al., 1957). From Fig. 5, the summer monthly 850-hPa horizontal winds in both reanalyses bear a consistency. For example, there are three branches of airflows with the southerly component across the equator: the strong southerly along coastal Somali, the southwesterly near 90°E, and the southeasterly near 120°E. These crossing-equator airflows develop and intensify

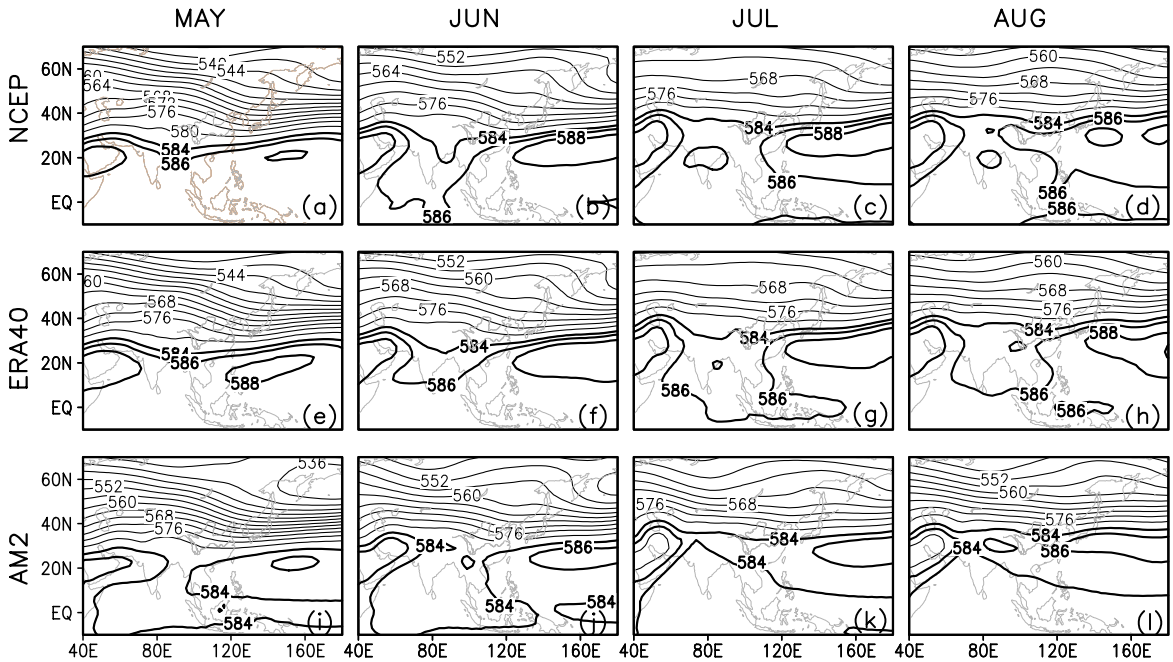

Fig. 4. Same as Fig. 3, but for 500-hPa. Contour intervals are 4 dagpm. The contour of 586 dagpm is displayed additionally.

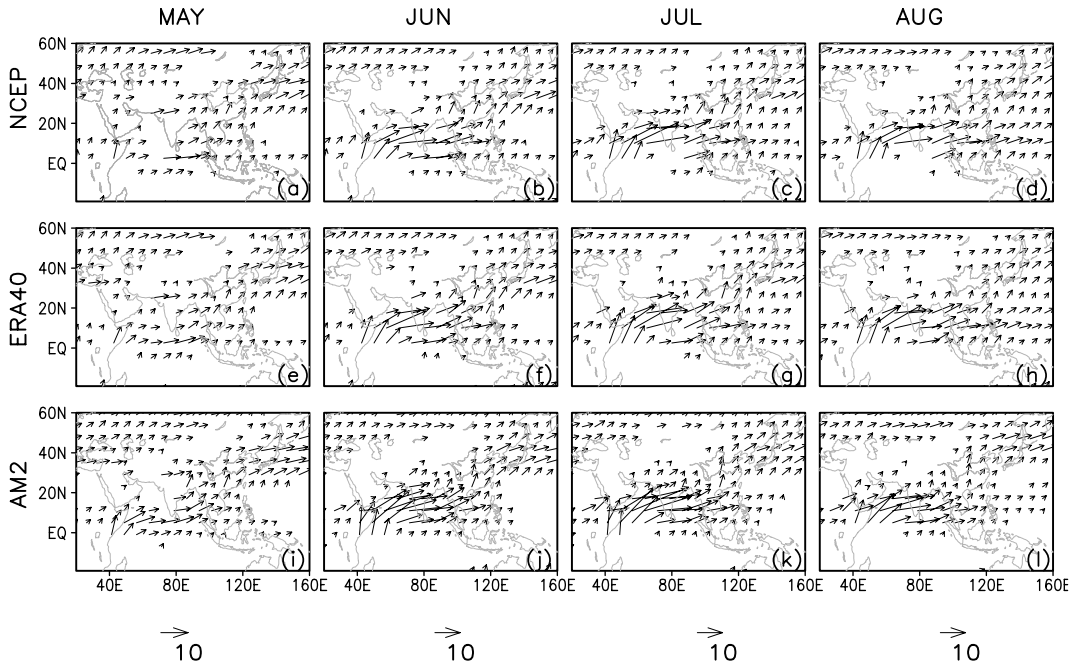

Fig. 5. Same as Fig. 2, but for the horizontal wind vectors at 850-hPa. Units: m s^{-1}. Only the winds with the amplitude greater than 1.0 m s^{-1} are shown for brevity.

along with the seasonal march of the EASM. The same features are seen in the AM2.

In summary, these validations suggest that the AM2 captures the primary features of the EASM and the associated atmospheric circulation evolution, which provide a solid base to understand the modeled responses.

4. Modeled interdecadal climate shift

4.1 *Rainfall*

From Fig. 6, there is a significant difference in July and August (JA) precipitation between the two sets of ensembles. In comparison with the first ensemble, which has climatological SST forcing averaged over 1950–69, the significantly enhanced precipitation is seen in the Yangtze River valley and sandwiched by the suppressed rainfalls in the south (coastal South China) and in the north (North China) in the second set of ensembles with climatological SST forcing from 1979–98. These anomalies are qualitatively in agreement with the observed climate shift between the two periods [cp. Fig. 6b with Fig. 6a, also with Fig. 1a in Huang (2001) and Fig. 4b in Zhao and Zhou (2006)], albeit a slight shift northward of the rainfall band and the marginal significance of the rainfall increase near the lower valley of the Yangtze River. Quantitatively, the observed interdecadal rainfall increase has the amplitude of about 1 mm d^{-1} (Fig. 6a), indicating an increase rate of about 20% given the observed climatological seasonal mean rainfall of 5 mm d^{-1} in the ERA-40 (Fig. 1). In the AM2, this increase has a value of about 0.6 mm d^{-1} also representing a rate of 20% or so given the AM2's climatological seasonal rainfall of 3 mm d^{-1}. This suggests that the observed interdecadal rainfall shift can be attributed to the global SST shift to a considerable extent.

Simulated surface air temperature in most of central China, especially in the lower reaches of the Yangtze River, is cooler with the maximum negative anomalies of 0.8, in accompany with warming in North China and coastal southern China. This is also consistent with the observed cooling trend of this area during the recent decades (cp. Fig. 6c and Fig. 6d, also see Zhou and Yu, 2006).

4.2 *Large-scale atmospheric circulation*

There are positive 100-hPa geopotential height anomalies in most of China but negative anomalies in the northeastern corner of China in the AM2 simulation (Fig. 7b). The anomalies correspond to the modeled precipitation increase and decrease shifts in the corresponding areas (Fig. 6). These anomalies are qualitatively consistent with the interdecadal variations in the ERA-40 reanalysis, albeit a shift of latitudinal location of the line of the contour 0. The observed interdecadal shift is calculated again as the mean of 1979–1998 minus the mean of 1950–69.

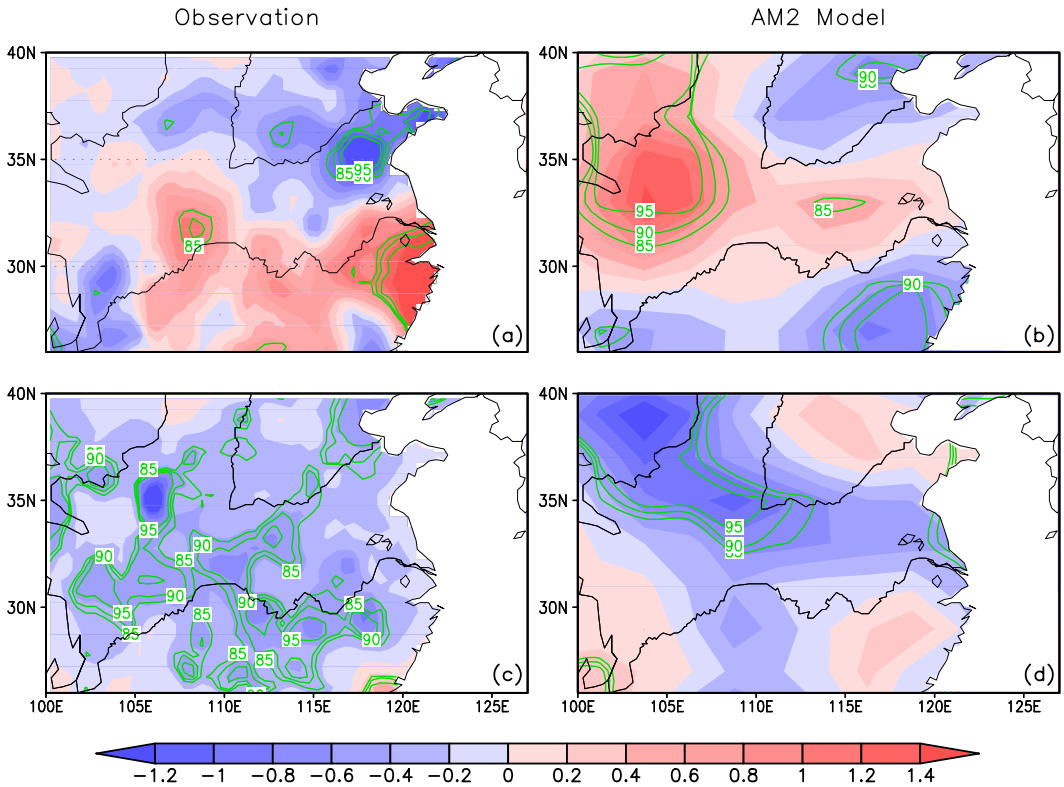

Fig. 6. Comparison of the AM2 simulated interdecadal anomalies of July-August mean precipitation (a, b, units: mm d^{-1}) and surface air temperature (c, d, units: °C) to the observed in the China 160-station dataset. The contours indicate the significance level.

The AM2 yields positive 500-hPa geopotential height anomalies to the south of 30°N along with negative anomalies to the north of 30°N (Fig. 7d). The anomalies indicate the westward stretching and the southward shift of the WPSH. This feature is seen in the ERA-40 reanalysis (Fig. 7a), which has been noted in the previous studies (e.g., Zhang et al., 2003; Ding et al., 2007; Zeng et al., 2007). To further clarify this point, Fig. 8 displays the comparison of the modeled 500-hPa geopotential height with those in the ERA-40. In observations, in the period of 1950–69 the characteristic ridge line with null westerly reflected by the west end of the contour line 586 reaches the middle reach of the Yangtze River (30°N, 115°E, Fig. 8a), but anchors at a southern location in the period of 1979–98 (25°N, 110°E, Fig. 8b). Correspondingly, one low encircled by the contour line of 584 is seen over the Indian Peninsula and BOB in the former period (Fig. 8a), but disappears in the latter period (Fig. 8b). These reflect that the observed WPSH stretches westward and shifts southward but intensifies after the late 1970s. In the model, the area encircled by the characteristic contour of 584 in the experiment forced with the SST climatology of the latter period is visually larger than in the experiment with the former SST climatology (cp. Figs. 8d with 8c). Also, the contour of 586 emerges in Fig. 8d. These suggest the modeled WPSH intensifies with the 1979–98 mean SST.

As far as the modeled 850-hPa wind field (Figs. 8e, f) is concerned, significant southwesterly anomalies are over the tropical Indian Ocean, the BOB, and the South China Sea, along with the southeasterly anomaly in the subtropical west Pacific and the easterly anomaly to the north of BOB and the Arabian Sea. In particular, there is a northerly anomaly in coastal eastern China, which reflects EASM weakening. These anomalies, particularly the anomalous northerly over eastern China, the reflector of EASM weakening, are qualitatively consistent with those in the ERA-40, and also with the previous studies (e.g., Wang, 2001; Han and Wang, 2007).

5. Summary and discussions

The AM2 simulating ability of the EASM is validated first, and it is found that the model reproduces EASM variability well. Then, ensemble experiments are conducted to explore the role of global SSTs in the interdecadal EASM shift which occurred around the late 1970s. The results indicate that the changes

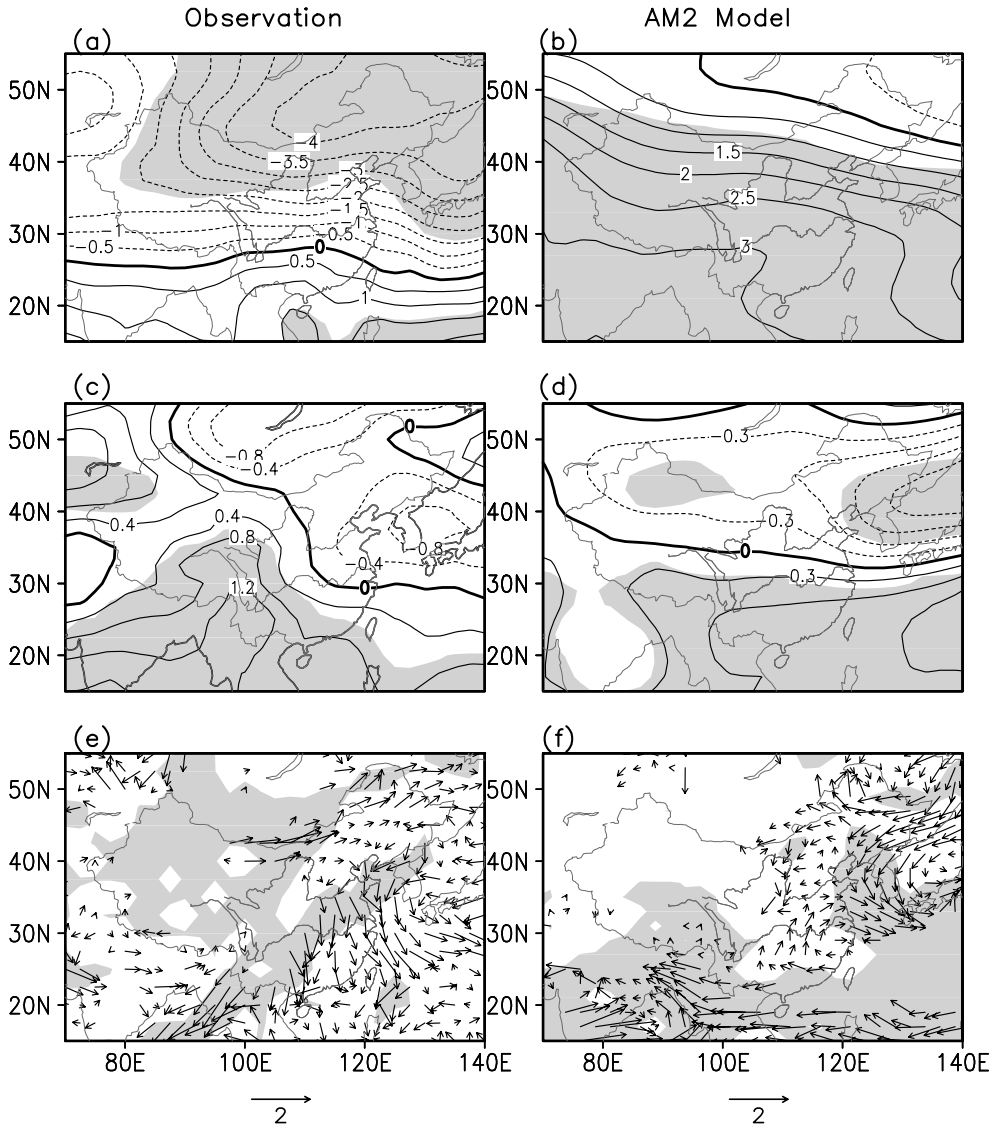

Fig. 7. Comparison of the AM2 simulated response to the interdecadal shift in the ERA-40. (a, b) and (c, d) are geopotential height (Units: dagpm) for 100-hPa and 500-hPa, respectively, and (e, f) are for 850-hPa horizontal wind vectors (Units: m s^{-1}). The shading indicates the significance level greater than 95%.

of climatological mean SST can qualitatively account for the East-Asian interdecadal climate shift and the associated atmospheric circulation change.

Previous studies suggest that the decadal SST variations in both the extratropical northern Pacific and the tropical Pacific SSTs may have contributed to the East Asian climate shift around the late 1970s (e.g., Huang, 2001; Gong and Ho, 2002; Yang et al., 2005; Ma, 2007). Our model results provide evidence for this possibility, although the influence of those different regional SSTs is not studied separately. Our results are consistent with the recent simulation in the NCAR CCM3 (Zeng et al., 2007), but inconsistent with Han and Wang (2007) who found that EASM interdecadal climate shift cannot be accounted for by the historical evolving global SST and sea ice concentration. Considering other natural factors like sea ice concentration, Tibetan Plateau and Eurasian snow cover may also play a role in this climate shift (e.g., Zhang and Tao, 2001; Zhao and Chen, 2001; Zhao et al., 2004), further studies using different AGCMs with different blended or isolated forcings are needed to figure out this issue.

The observed SST variation is composed of two components, one from the natural fluctuations of the climate system while the other from the signals of anthropogenic forcings. In our study, these two components are not separated from each other. Therefore, our results do not hint that the observed climate shift

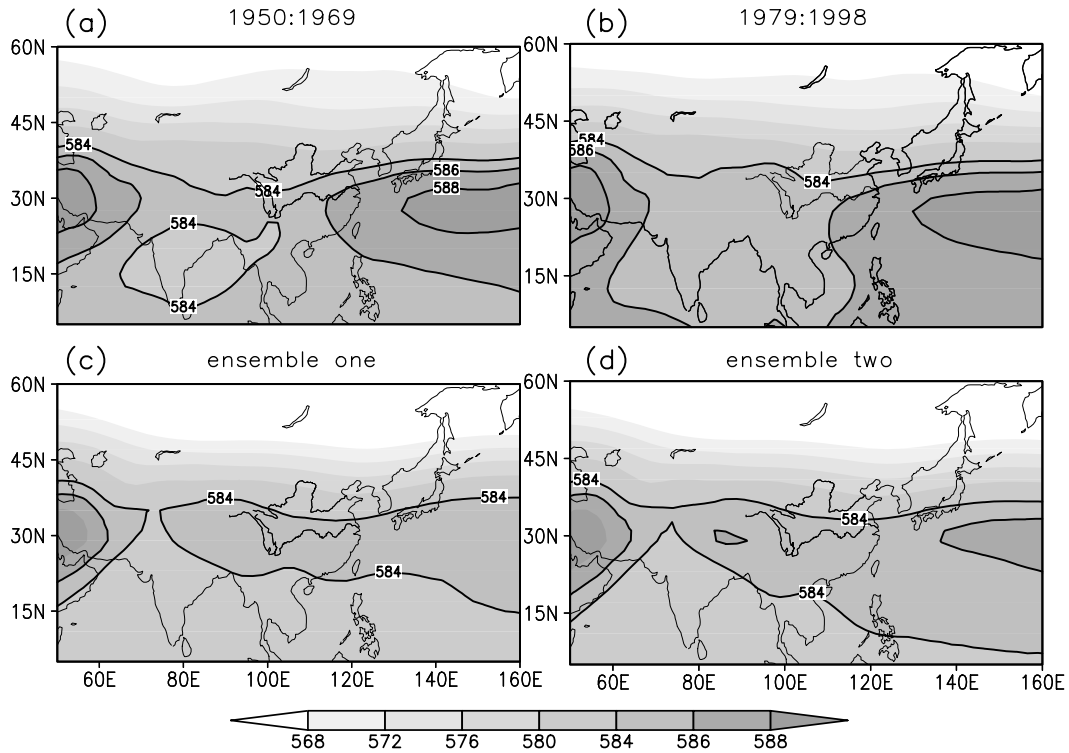

Fig. 8. Comparison of the AM2 simulated climatological July–August mean of 500-hPa geopotential height (c, d, units: dagpm) to that in the ERA-40 dataset. (a, b) Left panels correspond to the period of 1950–69 while right panels correspond to the period of 1979–98. Only the contours of 584, 586, and 588 are displayed.

is linked to the human forcing, although previous studies suggest that anthropogenic aerosols and greenhouse gases may indeed have had a role (Xu, 2001; Menon et al., 2002; Zhao et al., 2006). Besides, we only investigated the influence of the SST climatological mean rather than transient SSTs. Since SST transience may be important (e.g., Wang, 2002), further studies by forcing the AM2 with historical evolving SSTs may be helpful in solving this issue. At last, most of our analyses are qualitative, not quantitative, and a more comprehensive study is our future task.

Acknowledgements. The authors appreciate the two anonymous reviewers for their helpful suggestions. This study was jointly supported by the National Natural Science Foundation of China with Grant Nos. 90711004 and 40775053 and the Innovation Key Program (Grant Nos. KZCX2-YW-Q11-03 and KZCX2-YW-Q03-08) of the Chinese Academy of Sciences.

REFERENCES

Ding, Y., Z. Wang, and Y. Sun, 2007: Inter-decadal variation of the summer precipitation in East China and its association with decreasing Asian summer monsoon. Part I: Observed evidences. *International Journal of Climatology*, DOI: 10.1002/joc.1615.

GAMT (the GFDL global Atmospheric Model development Team), 2004: The new GFDL Atmosphere and Land Model AM2-LM2: Evaluation with prescribed SST simulations. *J. Climate*, **17**, 4641–4673.

Gong, D., and C. Ho, 2002: Shift in the summer rainfall over the Yangtze River valley in the late 1970s. *Geophys. Res. Lett.*, **29**(10), doi: 10.1007/00703-004-0081-z.

Han, J., and H. Wang, 2007: Interdecadal variability of East Asian summer monsoon in an AGCM model. *Adv. Atmos. Sci.*, **24**(5), 808–818. doi: 10.1007/s00376-007-0808-0.

Hoerling, M. P., J. W. Hurrell, T. Xu, G. T. Bates, and A. S. Phillips, 2004: Twentieth century North Atlantic climate change. Part II: Understanding the effect of Indian Ocean warming. *Climate Dyn.*, **23**, 391–405.

Huang, R., 2001: Decadal variability of the summer monsoon rainfall in East Asia and its association with the SST anomalies in the tropical Pacific. *CLIVAR Exchange*, **2**, 7–8.

Kalnay, E., and Coauthors, 1996: The NCEP/NCAR 40-year reanalysis project. *Bull. Amer. Meteor. Soc.*, **77**, 437–471.

Li, C., and P. Xian, 2003: Atmospheric anomalies related to interdecadal variability of SST in the North Pacific. *Adv. Atmos. Sci.*, **20**(6), 859–874.

Li, S., and G. Bates, 2007: Influence of the Atlantic Multidecadal Oscillation on the winter climate of

East China. *Adv. Atmos. Sci.*, **24**(1), 126–135. doi: 10.1007/s00376-007-0126-6.

Lu, R., and B. Dong, 2005: Impact of Atlantic sea surface temperature anomalies on the summer climate in the western North Pacific during 1997–1998. *J. Geophys. Res.*, **110**, D16102, doi: 10.1029/2004JD005676.

Lu, R., B. Dong, and H. Ding, 2006: Impact of the Atlantic Multidecadal Oscillation on the Asian summer monsoon. *Geophys. Res. Lett.*, **33**, L24701, doi:10.1029/2006GL027655.

Ma, Z., 2007: The interdecadal trend and shift of dry/wet over the central part of North China and their relationship to the Pacific decadal oscillation. *Chinese Science Bulletin*, **52**(15), 2130–2139.

Menon, S., J. Hansen, L. Nazarenko, and Y. F. Luo, 2002: Climate effects of black carbon aerosols in China and India. *Science*, **297**, 2250–2253.

Nitta, T., and S. Yamada, 1989: Recent warming of tropical sea surface temperature and its relationship to the Northern Hemisphere circulation. *J. Meteor. Soc. Japan*, **67**, 375–383.

Rayner, N. A., E. B. Horton, D. E. Parker, C. K. Folland, and R. B. Hackett., 1996: Version 2.2 of the global sea surface temperature data set, 1903–1994. Climate Research Technical Note 74, Hadley Center for Climate Prediction and Research, UK Meteorological Office.

Renwick, J, A., 2002: Southern Hemispheric circulation and relations with sea ice and sea surface temperatures. *J. Climate*, **15**, 3058–3068.

Tao, S., and Staff Members of Academia Sinica, 1957: On the general circulation over the Eastern Asia I. *Tellus*, **9**, 432–446.

Upplal, S., and Coauthors, 2004: ERA-40: ECMWF 45-years reanalysis of the global atmosphere and surface conditions 1957–2001. *ECMWF Newsletter Meteorology*, **101**, 2–21.

Wang, H., 2001: The weakening of the Asian monsoon circulation after the end of 1970s. *Adv. Atmos. Sci.*, **18**, 376–386.

Wang, H., 2002: The instability of the East Asian Summer Monsoon-ENSO relations. *Adv. Atmos. Sci.*, **19**, 1–11.

Wu, B., and R. Zhang, 2007: Interdecadal shift in the western North Pacific summer SST anomaly in the late 1980s. *Chinese Science Bulletin*, **52**(18), 2559–2564.

Xie, P., and P. A. Arkin, 1997: Global precipitation: A 17-year monthly analysis based on gauge observations, satellite estimates and numerical model outputs. *Bull. Amer. Meteor. Soc.*, **78**, 2539–2558.

Xu, Q., 2001: Abrupt change of the mid-summer climate in central east China by the influence of atmospheric pollution. *Atmos. Environ.*, **35**, 5029–5040.

Yang, H., and Q. Zhang, 2003: On the decadal and interdecadal variability in the Pacific Ocean. *Adv. Atmos. Sci.*, **20**(2), 173–184.

Yang, J., Q. Liu, S. Xie, Z. Liu, and L. Wu, 2007: Impact of the Indian Ocean SST basin mode on the Asian summer monsoon. *Geophys. Res. Lett.*, **34**, L02708, doi: 10.1029/2006GL028571.

Yang, X., Q. Xie, Y. Zhu, X. Sun, and Y. Guo, 2005: Decadal-to-interdecadal variability of precipitation in North China and associated atmospheric and oceanic anomaly patterns. *Chinese Journal of Geophysics*, **48**(4), 789–797. (in Chinese)

Zeng, G., Z. Sun, W. Wang, and J. Min, 2007: Interdecadal variability of the East Asian summer monsoon and associated atmospheric circulations. *Adv. Atmos. Sci.*, **24**(5), 915–926. doi: 10.1007/s00376-007-0915-y.

Zeng, G., Z. Sun, W. Wang, Z. Lin, and D. Ni, 2007: Interdecadal variation of East Asian summer monsoon Simulated by NCAR Cam3 driven by global SSTs. *Climatic and Environmental Research*, **12**(2), 211–224. (in Chinese)

Zhang, Q., J. Wei, and S. Tao, 2003: Interannual and interdecadal variations of North China drought and associated atmospheric circulation in the recent 50 years. *Climatic and Environmental Research*, **8**(3), 307–318. (in Chinese)

Zhang, S., and S. Tao, 2001: Diagnostics and modeling on the influence of Tibetan Plateau accumulated snow upon Asian summer monsoon. *Acta Meteorologica Sinica*, **25**(3), 372–390. (in Chinese)

Zhang, Y., J. M. Wallace, and D. S. Battisti, 1997: ENSO-like interdecadal variability: 1900–93. *J. Climate*, **10**, 1004–1020.

Zhao, C., X. Tie, and Y. Lin, 2006: A possible positive feedback of reduction of precipitation and increase in aerosols over eastern central China. *Geophys. Res. Lett.*, **33**, L11814, doi: 10.1029/2006GL025959

Zhao, P., and L. Chen, 2001: Interannual variability of atmospheric heat source/sink over the Qinghai-Xizang (Tibetan) Plateau and its relation to circulation. *Adv. Atmos. Sci.*, **18**(1), 106–116.

Zhao, P., and X. Zhou, 2006: Decadal variability of rainfall persistence time and rainbelt shift over Eastern China in recent 40 years. *Journal of Applied Meteorological Science*, **17**(5), 548–556. (in Chinese)

Zhao, P., X. Zhang, X. Zhou, M. Ikeda, and Y. Yin, 2004: The sea ice extent anomaly in the North Pacific and its impact on the East Asian summer monsoon rainfall. *J. Climate*, **17**, 3434–3447.

Zhou, T., and R. Yu, 2006: Twentieth-century surface air temperature over China and the globe simulated by coupled climate models. *J. Climate*, **19**, 5843–5858.